

## Superionicity of $\text{H}^{\delta-}$ in $\text{LaH}_{10}$ superhydride

Maélie Causse<sup>1,\*</sup>, Grégory Geneste<sup>1,†</sup> and Paul Loubeyre<sup>1,‡</sup>  
 CEA, DAM, DIF, 91297 Arpajon Cedex, France and Université Paris-Saclay, CEA,  
 Laboratoire Matière en Conditions Extrêmes, 91680 Bruyères le Châtel, France

(Received 3 July 2022; revised 12 September 2022; accepted 16 December 2022; published 1 February 2023)

Recent computational studies have successfully predicted the dramatic uptake of hydrogen by metals under pressure leading to the formation of superhydrides, now ubiquitously observed.  $\text{LaH}_{10}$  exemplifies the properties of these novel H-rich compounds, some of which form a novel class of superconducting materials. We show here another remarkable property for superhydrides, namely,  $\text{H}^{\delta-}$  superionicity. By means of *ab initio* molecular dynamics simulations in  $\text{LaH}_{10}$ , an exceptionally high hydride ( $\text{H}^{\delta-}$ ) diffusion coefficient is calculated at high temperature, with  $D = 1.7 \times 10^{-4} \text{ cm}^2/\text{s}$  at 170 GPa and 1500 K, corresponding to an ionic conductivity of  $\sigma = 0.9 (\Omega \text{ cm})^{-1}$  and so indicating a superionic phase. The superionic phase is surprisingly stable up to 2500 K and its melting temperature is remarkably high, similar to that of pure La. The connected path for the hydride ionic diffusion is disclosed, with the H sublattice keeping its clathrate structure. The conductivity properties of  $\text{LaH}_{10}$  are discussed in relation to the recently discovered family of compounds showing fast pure hydride ions transport.

DOI: [10.1103/PhysRevB.107.L060301](https://doi.org/10.1103/PhysRevB.107.L060301)

**Introduction.** High pressure promotes the formation of novel polyhydrides with unusually high hydrogen-to-metal ratio, called superhydrides [1,2]. They can be viewed as additive volume alloys between metal hydrogen and a metal [3]. Some remarkable properties of metal hydrogen are thus expected to exist in these superhydrides, such as a high-temperature superconductivity [4] or a high-H diffusion [5]. Indeed, some superhydrides, in particular those made of rare-earth elements, probably form a novel class of conventional superconducting materials, with high critical temperatures [6]. These compounds exhibit very particular crystal structures, called “hydrogen clathrates” [7], in which the hydrogen sublattice is reminiscent of the structure of metal hydrogen [8] and forms cages in which metal atoms are inserted.  $\text{LaH}_{10}$  is a remarkable example of this novel class of polyhydride compounds [9,10].  $\text{LaH}_{10}$  displays a very high superconducting critical temperature ( $T_c$ ) of 250 K at  $\sim 170\text{--}200$  GPa [11,12]. Recently, it has been suggested, based on an emerging hydrogen diffusion at 800 K and 150 GPa [8], that  $\text{LaH}_{10}$  may enter a superionic phase under high pressure. Here, we further investigate such a possibility by addressing the following questions: Can the H diffusion coefficient reach the high value needed for qualifying a superionic phase? Is the H atom’s fast diffusion associated to a melting of the H sublattice and can  $\text{LaH}_{10}$  be stable under such conditions? How does the hydride ion’s ( $\text{H}^{\delta-}$ ) conductivity in  $\text{LaH}_{10}$  compare to those of recently discovered hydride ionic conductors?

**Methods.** We performed *ab initio* molecular dynamics (AIMD) simulations on  $\text{LaH}_{10}$  with the ABINIT code [13], using the Generalized Gradient Approximation as formulated

by Perdew, Burke and Ernzerhof (GGA-PBE) [14], in the framework of the projector augmented-wave (PAW) method [15,16]. Two kinds of AIMD trajectories were generated: (i) A first set in the canonical (NVT) ensemble, using the Langevin thermostat for the thermalization and by setting the same mass to the La and H atoms, ensuring efficient sampling of the NVT ensemble, but the loss of the physical meaning of time [17–21]; (ii) a second set using the true masses for La and H, in the microcanonical (NVE) ensemble. From the first set of trajectories, we extract static thermodynamic quantities (pair distribution functions, atomic densities), while from the second one, we get the mean-square displacements as a function of time, and thus the diffusion coefficient (see Supplemental Material [22]). An isochoric path was followed by increasing the temperature from 600 to 3000 K with the associated pressure evolving from 156 to 187 GPa. Simulations were performed using a  $2 \times 2 \times 2$  supercell in terms of the conventional fcc unit cell of  $\text{LaH}_{10}$  (with periodic boundary conditions applied in the three directions), leading to 352 atom-supercells. A time step of  $\sim 0.25$  fs, suitable for the study of hydrogen dynamics, was used for the discretization of the Newton’s equations of motion, which are integrated within the Verlet algorithm. An AIMD trajectory using a  $3 \times 3 \times 3$  supercell (1188 atoms) was also performed at 2000 K to test the sensitivity of the simulations to finite-size effects.

Within the GGA-PBE, it was previously established that the fcc- $\text{LaH}_{10}$  phase exhibits a dynamical instability at  $T = 0$  K below 210 GPa [8,10]. However, this dynamical instability is suppressed when nuclear quantum effects are taken into account, indicating that the fcc phase is the true ground state at those pressures [23]. Thermal fluctuations act similarly as nuclear quantum effects and favor the stability of the  $Fm\bar{3}m$  structure at high temperature [24], which justifies the use of the cubic structure as the starting point of the present simulations. Bader charge analysis was performed on the perfect fcc

\*maelie.causse@cea.fr

†gregory.geneste@cea.fr

‡paul.loubeyre@cea.fr

structure to determine the charge transfer between La and H atoms: the charge transfer is calculated to be nonequivalent for the H atoms sitting on the octahedral ( $H_o$ ) and tetrahedral ( $H_t$ ) sites, with  $\sim -0.15e$  and  $-0.01e$  per H atom, respectively. The La atom is positively charged with  $\sim 1.2e$ . Note that the negative charge on H atoms confirms that  $\text{LaH}_{10}$  is a hydride, and that the values computed by the Bader method are rather far from the formal charges, especially for La. However, similar charge transfers are obtained by the same method in other superhydrides such as manganese [25] (Mn charge  $\sim +0.3$ – $0.6e$ ) and iron [26] (Fe charge  $\sim +0.2$ – $0.4e$ ) superhydrides under high pressure. That is also similar to the charge transfer previously calculated from a Mulliken population analysis in various rare-earth superhydrides (La charge around  $+1.6$ – $1.7$  for  $\text{LaH}_6$  [7]).

**Superionic phase.** At 600 K (and 156 GPa),  $\text{LaH}_{10}$  is a solid with no intrinsic diffusion, with La and H atoms only vibrating around their mean lattice positions. At 1000 K (and 163 GPa), the H atoms are observed to diffuse over the 1 ps timescale of the simulation. The mean-square displacement (MSD)  $\langle \Delta r^2 \rangle$ , averaged over all H atoms, is calculated and the H diffusion coefficient is then derived using the relation  $\langle \Delta r^2 \rangle = 6D_H t$ , under the assumption of a three-dimensional random walk. In Fig. 1(a), the MSD is plotted versus time at various temperatures, and quasilinear curves are obtained, as expected from a diffusive regime, with the diffusion coefficient being directly related to the slope. At 1000 K (and 163 GPa),  $D_H = 3.2 \times 10^{-5} \text{ cm}^2/\text{s}$ . A dramatic increase of the diffusion constant is observed at higher temperatures, reaching  $D_H = 6.9 \times 10^{-4} \text{ cm}^2/\text{s}$  at 2500 K (and 183 GPa). Despite high diffusion of the H atoms, the La atoms remain vibrating on their fcc lattice sites. A melting of the La sublattice is observed at 3000 K, suggesting that the melting temperature along the isochoric path should be between 2500 and 3000 K. The diffusion coefficient is plotted in Fig. 1(b) using an Arrhenius representation: we observe that the logarithm of  $D$  evolves linearly as a function of the inverse temperature, indicating an Arrhenius behavior. The diffusion coefficient can so be expressed as

$$D_H = D_0 e^{-\frac{E_a}{k_B T}}, \quad \text{with } D_0 \sim a^2 \nu, \quad (1)$$

where  $E_a$  is the activation energy,  $a$  the hopping distance, and  $\nu$  the *attempt* frequency which can provide information about the hopping mechanism. The linear fit in Fig. 1(b) yields  $D_0 = 5.1 \times 10^{-3} \text{ cm}^2/\text{s}$ ,  $E_a = 0.44 \text{ eV}$ , and  $\nu \sim 42.4 \text{ THz}$ . It is assumed that  $E_a$  and  $\nu$  do not strongly depend on the pressure between  $\sim 160$  and  $180 \text{ GPa}$ . The high value of  $\nu$ , of similar magnitude as those of the highest-frequency phonon modes in  $C2/m$ - $\text{LaH}_{10}$  (which correspond to vibrations of hydrogen atoms [8]) or that of the  $\text{H}_2$  vibron (about  $122 \text{ THz}$ ) indicates that H hopping is driven by the thermal vibrations of the H atoms, rather than by those of the La sublattice.

Superionic conductors are solid materials that display very high ionic conductivities, about  $1 (\Omega \text{ cm})^{-1}$ , associated to an ionic diffusion coefficient  $D$  about  $\sim 10^{-5} \text{ cm}^2/\text{s}$ , as those typically found in molten salts [27].  $\text{LaH}_{10}$  enters a superionic phase at about 1500 K since there, as it will be seen below, the associated value of the ionic conductivity is becoming greater than  $1 (\Omega \text{ cm})^{-1}$ . There exist three types of transitions, from

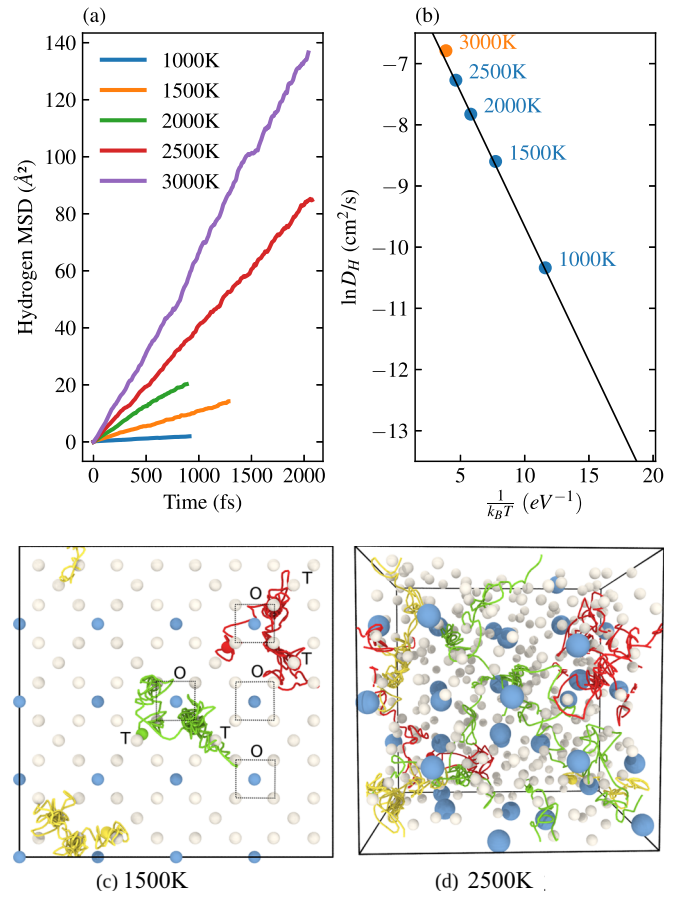


FIG. 1. Dynamical behaviors of hydrogen atoms in  $\text{LaH}_{10}$  at high temperatures and  $\sim 170 \text{ GPa}$ . (a) MSD of H at different temperatures. (b) The associated diffusion coefficient is plotted in an Arrhenius representation (as blue and orange dots for solid and fluid phases). (c),(d) Diffusion paths of H atoms in fcc  $\text{LaH}_{10}$ . Red, yellow, and green lines correspond to the trajectories of three selected H atoms during the 1.32 and 2.15 ps AIMD run at 1500 and 2500 K, respectively. Lanthanum and hydrogen atoms are represented as blue spheres and gray circles, respectively. In (c), the three trajectories of H at 1500 K are superimposed to the perfect cubic structure at 0 K and octahedral (O) and tetrahedral (T) sites are outlined.

a low-temperature ion insulating phase to a high-temperature superionic phase, essentially based on the evolution of conductivity (or diffusion) versus temperature [27]. A type-III superionic transition is observed here for  $\text{LaH}_{10}$  since the high ionic conductivity state is developing with temperature in a smooth fashion, following an Arrhenius behavior, with no change of slope or discontinuity. Extrapolating the linear fit of Fig. 1(b) down to 600 K gives a diffusion coefficient  $D_H = 1.1 \times 10^{-6} \text{ cm}^2/\text{s}$ , which could not be characterized over the ps timescale of the simulation. We also performed path-integral molecular dynamics simulations at 600 K to check whether nuclear quantum effects could significantly enhance H diffusion, but no diffusion was detected within the timescale of the calculation (see Supplemental Material [22]). It should be noted that the calculated diffusion coefficient at 3000 K is above the linear fit, confirming the melting of  $\text{LaH}_{10}$ , which was characterized from the disordering of the La sublattice (see Supplemental Material [22]).

**Mechanism of H diffusion.** The H atom's diffusion is visualized at the atomic scale in Figs. 1(c) and 1(d) by following the trajectories of three selected H atoms, over the 2 ps simulation time. At 1500 K, a clear connected path is disclosed. The H atom diffusion remains constrained on the underlying H-backbone sublattice, with connected 8-hydrogen-atom cubic units (on octahedral sites) and unit H atoms (on tetrahedral sites). The H atoms rotationally diffuse on the octahedral site cubic unit, jump to the next tetrahedral H unit, and, from there, jump to another octahedral site cubic unit. At 2500 K, this mechanism is fast enough so that long diffusion paths outside the simulation box are observed over 1 ps. The atomic diffusion in a superionic conductor, whose ground state is perfectly ordered, is usually rationalized in terms of point defects forming Frenkel pairs. When the value of the (positive) formation energy of a defect is much larger than the value of the (negative) energy of the interaction between two defects, an Arrhenius behavior for the concentration of mobile ions is observed, i.e., qualifying a type-III superionic conductor [27], as here for  $LaH_{10}$ . One particular atomic defect was pointed out by the structural optimization of configurations of the lanthanum superhydride compound in the diffusive state at 1000 K, as showed in Fig. 2(a). When an H atom jumps from the octahedral  $H_8$  unit to an occupied H-unit tetrahedral site, the two H atoms form a metastable dimer with a H-H distance equal to  $\sim 1.37$  Å, which can sit on the tetrahedral site (see Supplemental Material [22]).

The endurance of the H sublattice in the superionic phase up to the melting of  $LaH_{10}$  is also observed by scrutinizing the atomic hydrogen density distribution over the simulations, and by plotting the pair distribution function (PDF) of the H atoms (Fig. 2). The backbone-H structure remains, although it is more and more blurred by dynamical disorder as it approaches melting. At 600 K, the H atom's PDF is structured with the thermal broadening of the Dirac peaks of the PDF in the solid at 0 K. The H atom's PDF,  $G(r)$ , is drastically changing upon entering the superionic phase about 1500 K, by adopting a more liquidlike shape. However, a plateau of  $G(r)$  in between  $\sim 1.1$  Å and  $\sim 1.8$  Å cannot be explained by that of a simple liquid PDF. That is another piece of evidence that the H atoms diffuse on the clathrate-H sublattice. By tagging H atoms with their position at the start of the simulation either as being tetrahedral or octahedral if sitting on the respective interstitial sites of the fcc La sublattice, the partial PDF  $H_t-H_t$  and  $H_o-H_o$  corresponding to the two subfamilies of tetrahedral and octahedral H atoms are obtained, as shown in the Supplemental Material [22]. Upon entering the superionic regime, the diffusion of the H atoms blurs the difference between the PDF  $H_t-H_t$  and PDF  $H_o-H_o$ . At 2500 K, due to the extremely fast diffusion, the memory of the initial H position is completely lost and the two partial H PDFs are identical. Note that the AIMD trajectory performed using a  $3 \times 3 \times 3$  supercell (1188 atoms) at 2000 K did not evidence any size effects artifact on the PDF (see Supplemental Material [22]).

**High hydride ionic conductivity.** The ionic conductivity  $\sigma$  associated to the hydride diffusion through the  $LaH_{10}$  lattice is calculated using the Nernst-Einstein formula,

$$\sigma = \frac{[H^{\delta-}]Z_{H^{\delta-}}^2 D_H}{k_B T}, \quad (2)$$

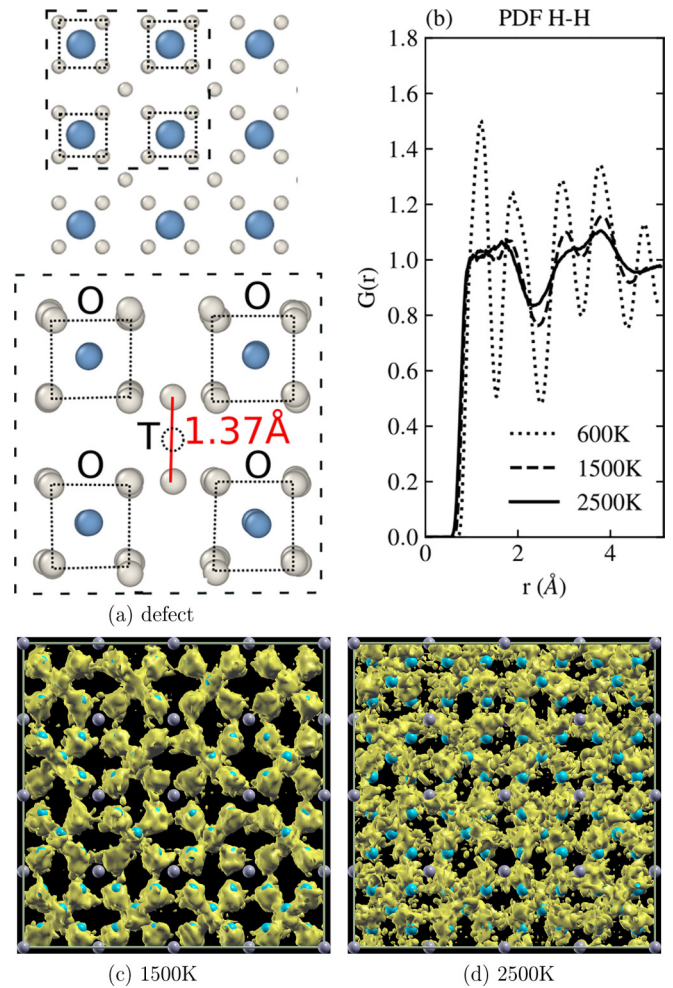


FIG. 2. Mechanism of the H diffusion. (a) Defect formation in the fcc  $LaH_{10}$  enabling the H diffusion. The fcc- $LaH_{10}$  perfect crystal is drawn with 8H-cube octahedral sites and H tetrahedral sites. Each lanthanum (blue) atom is surrounded by a 32H-clathrate cage. The defect (in red) consists of an extra hydrogen atom which sits on a T interstitial site. (b) Change of the H-H PDF with temperature. (c),(d) Isosurface of the density of probability of hydrogen atoms (yellow) at two temperatures (1500 and 2500 K) overlap the fcc- $LaH_{10}$  lattice at 0 K (isovalue 1.1 atoms/Å<sup>3</sup>). Lanthanum and hydrogen positions of the perfect fcc crystal are indicated by gray and blue dots, respectively. Remarkably, hydrogen diffusion paths are on the clathrate lattice in the superionic phase at 1500 and 2500 K.

where  $[H^{\delta-}]$  is the concentration of  $H^{\delta-}$  ions,  $Z_{H^{\delta-}}$  their electric charge, and  $D_H$  their diffusion coefficient. The electric charge on the H atoms is estimated from the Bader charge analysis obtained using the perfect fcc- $LaH_{10}$  lattice, namely,  $-0.15e$  and  $-0.01e$  per H atom sitting on the octahedral and tetrahedral sites, respectively. The value taken for  $Z_{H^{\delta-}}$  is the average of these two values, weighted by the corresponding populations of the two sites at  $T = 0$  K, i.e.,  $4/5$  for  $H_o$  and  $1/5$  for  $H_t$ . The ionic conductivity evolves from  $0.25$  ( $\Omega$  cm)<sup>-1</sup> to  $0.90$  ( $\Omega$  cm)<sup>-1</sup> by going from 1000 to 1500 K. The accepted conductivity threshold for superionicity being  $1$  ( $\Omega$  cm)<sup>-1</sup> [27],  $LaH_{10}$  hence enters its superionic phase at about 1500 K. It is interesting to note that the electronic density of states is almost not changing with

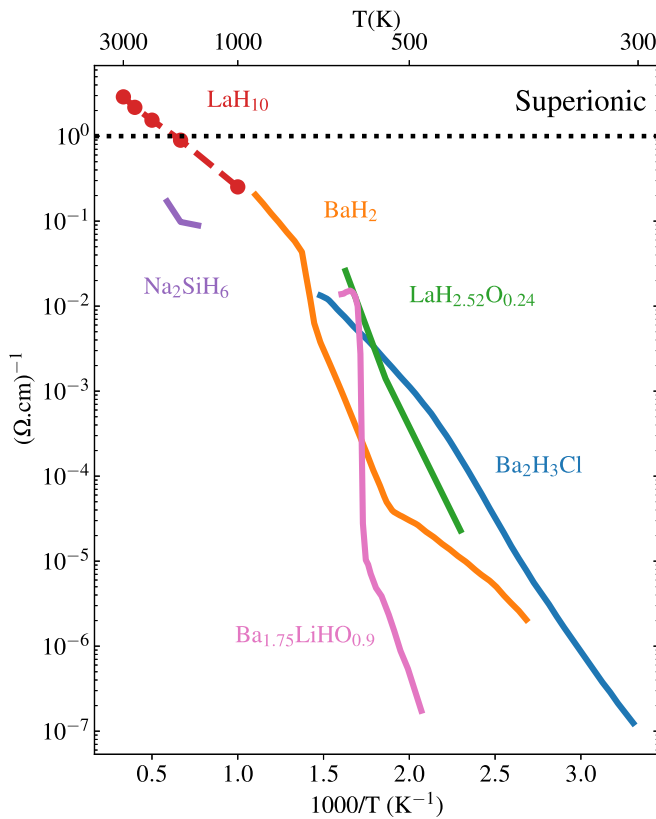


FIG. 3. Comparison of ionic hydride conductivities in  $\text{LaH}_{10}$  (at high temperatures, in red) and in other ionic conductors. Shown are  $\text{BaH}_2$  [30],  $\text{Ba}_{1.75}\text{LiHO}_{0.9}$  [33],  $\text{Ba}_2\text{H}_3\text{Cl}$  [32],  $\text{LaH}_{2.52}\text{O}_{0.24}$  [31], and  $\text{Na}_2\text{SiH}_6$  [34].

temperature (see Supplemental Material [22]), and hence  $\text{LaH}_{10}$  can be viewed as a superionic metal.

The study of materials exhibiting fast hydrogen transport has attracted great interest for a wide range of applications such as H-storage materials and electrochemical devices [28–32]. Barium hydride was the first material to demonstrate a fast pure hydride ( $\text{H}^-$ ) conductivity in its high-temperature high-symmetry phase, not yet reaching values expected for a superionic phase [30]. Figure 3 shows an Arrhenius plot of the hydride ionic conductivity of  $\text{LaH}_{10}$  which is compared to those of other hydride conductors.  $\text{BaH}_2$  was the first material to exhibit pure hydride ionic transport, with a conductivity in its high-temperature symmetric phase an order of magnitude higher than that typical of proton conductors [30]. It was then found that by stabilizing the symmetric phase of

$\text{BaH}_2$  at low temperature through ordered anion substitution with halide ions, remarkable hydride conductivity could be achieved even at room temperature, such as in  $\text{Ba}_2\text{H}_3\text{Cl}$  [32]. The hydride conductivity in oxyhydrides has also been investigated. High conductivity at intermediate temperature has been obtained in  $\text{LaH}_{2.52}\text{O}_{0.24}$  [31]. Adding chemical complexity, a high-temperature-independent hydride conductivity was observed in  $\text{Ba}_{1.75}\text{LiHO}_{0.9}$  [33]. The conductivity in  $\text{LaH}_{10}$  is in agreement with the extrapolation to high temperature of the behavior of these ambient pressure hydride ion conductors. The activation energies for conductivity in these various compounds are thus similar despite different mechanisms for  $\text{H}^-$  diffusion. Superionicity is observed here because of the stability of  $\text{LaH}_{10}$  at higher temperatures. Recently, the stability of a hydride ( $\text{H}^-$ ) superionic phase was predicted under pressure by *ab initio* molecular dynamics (AIMD) in sodium silicon hydride  $\text{Na}_2\text{SiH}_6$  [34], but, as seen in Fig. 3, its hydride conductivity is below this common trend and below the superionic transition criteria.

Another remarkable property of the superionic phase in  $\text{LaH}_{10}$  is its thermodynamic stability. Around 160 GPa, the melting temperature of solid hydrogen has been measured at about 800 K [35]. The melting line of La has been measured up to 4 GPa only [36] and the bold linear extrapolation of the known experimental melting line gives an upper bound about 3500 K for the La melting point at 160 GPa. Assuming an ideal mixing between these two elements, the melting point of  $\text{LaH}_{10}$  would be expected around 1250 K. It is observed here about 3000 K. That is analogous to the sharp increase of slope of the melting line of ice when entering its proton superionic phase [37,38].

*Conclusion.* A remarkable property is revealed in  $\text{LaH}_{10}$ , namely, the hydride superionic conductivity. Such a property might also exist in other superhydrides. The current strategy for the rational design of superhydrides at low pressure [39] could hence lead to materials with remarkably fast hydride ions transport. The experimental validation of such a superionic state is a challenge that might be tackled directly by measuring the diffusion of hydrogen using nuclear magnetic resonance (NMR) at high pressure [40] or indirectly by observing the high melting temperature of  $\text{LaH}_{10}$ , or its thermal expansion becoming discontinuously larger in the superionic phase (see Supplemental Material [22]).

*Acknowledgments.* M.C. would like to thank Romuald Béjaud and Paul Lafourcade for their help using the OVITO software [41], with which Figs. 1(c) and 1(d) have been done. Figures 2(c) and 2(d) have been done using the XCrySDen program [42].

- [1] E. Zurek, *Comments Inorgan. Chem.* **37**, 78 (2017).
- [2] M. Du, W. Zhao, T. Cui, and D. Duan, *J. Phys.: Condens. Matter* **34**, 173001 (2022).
- [3] B. Guigue, A. Marizy, and P. Loubeyre, *Phys. Rev. B* **102**, 014107 (2020).
- [4] N. W. Ashcroft, *Phys. Rev. Lett.* **21**, 1748 (1968).

- [5] H. Y. Geng, Q. Wu, and Y. Sun, *J. Phys. Chem. Lett.* **8**, 223 (2017).
- [6] J. A. Flores-Livas, L. Boeri, A. Sanna, G. Profeta, R. Arita, and M. Eremets, *Phys. Rep.* **856**, 1 (2020).
- [7] F. Peng, Y. Sun, C. J. Pickard, R. J. Needs, Q. Wu, and Y. Ma, *Phys. Rev. Lett.* **119**, 107001 (2017).

- [8] H. Liu, I. I. Naumov, Z. M. Geballe, M. Somayazulu, J. S. Tse, and R. J. Hemley, *Phys. Rev. B* **98**, 100102(R) (2018).
- [9] Z. M. Geballe, H. Liu, A. K. Mishra, M. Ahart, M. Somayazulu, Y. Meng, M. Baldini, and R. J. Hemley, *Angew. Chem. Int. Ed.* **57**, 688 (2018).
- [10] H. Liu, I. I. Naumov, R. Hoffmann, N. W. Ashcroft, and R. J. Hemley, *Proc. Natl. Acad. Sci. USA* **114**, 6990 (2017).
- [11] M. Somayazulu, M. Ahart, A. K. Mishra, Z. M. Geballe, M. Baldini, Y. Meng, V. V. Struzhkin, and R. J. Hemley, *Phys. Rev. Lett.* **122**, 027001 (2019).
- [12] A. P. Drozdov, P. P. Kong, V. S. Minkov, S. P. Besedin, M. A. Kuzovnikov, S. Mozaffari, D. A. Balicas, M. Tkacz, and M. I. Erements, *Nature (London)* **569**, 528 (2019).
- [13] X. Gonze, F. Jollet, F. Abreu Araujo, D. Adams, B. Amadon, T. Applencourt, C. Audouze, J.-M. Beuken, J. Bieder, A. Bokhanchuk, E. Bousquet, F. Bruneval, D. Caliste, M. Côté, F. Dahm, F. Da Pieve, M. Delaveau, M. Di Gennaro, B. Dorado, C. Espejo *et al.*, *Comput. Phys. Commun.* **205**, 106 (2016).
- [14] J. P. Perdew, K. Burke, and M. Ernzerhof, *Phys. Rev. Lett.* **77**, 3865 (1996).
- [15] P. E. Blöchl, *Phys. Rev. B* **50**, 17953 (1994).
- [16] M. Torrent, F. Jollet, F. Bottin, G. Zérah, and X. Gonze, *Comput. Mater. Sci.* **42**, 337 (2008).
- [17] C. H. Bennett, *J. Comput. Phys.* **19**, 267 (1975).
- [18] R. Pomés and J. McCammon, *Chem. Phys. Lett.* **166**, 425 (1990).
- [19] Y.-P. Pang, *Biochem. Biophys. Rep.* **4**, 126 (2015).
- [20] C. W. Hopkins, S. Le Grand, R. C. Walker, and A. E. Roitberg, *J. Chem. Theory Comput.* **11**, 1864 (2015).
- [21] J.-F. Danel and L. Kazandjian, *Phys. Plasmas* **25**, 060702 (2018).
- [22] See Supplemental Material at <http://link.aps.org/supplemental/10.1103/PhysRevB.107.L060301> for calculated Bader charges, atomic mean-square displacements, diffusion coefficients, pair distribution functions, electronic densities of states and volume expansion of LaH<sub>10</sub>.
- [23] I. Errea, F. Belli, L. Monacelli, A. Sanna, T. Koretsune, T. Tadano, R. Bianco, M. Calandra, R. Arita, F. Mauri, and J. A. Flores-Livas, *Nature (London)* **578**, 66 (2020).
- [24] Y. Watanabe, T. Nomoto, and R. Arita, *Phys. Rev. B* **105**, 174111 (2022).
- [25] J.-B. Charraud, G. Geneste, and M. Torrent, *Phys. Rev. B* **100**, 224102 (2019).
- [26] S. Zhang, J. Lin, Y. Wang, G. Yang, A. Bergara, and Y. Ma, *J. Phys. Chem. C* **122**, 12022 (2018).
- [27] J. Boyce and B. Huberman, *Phys. Rep.* **51**, 189 (1979).
- [28] K. Kreuer, *Annu. Rev. Mater. Res.* **33**, 333 (2003).
- [29] K. Kamazawa, M. Harada, T. Araki, Y. Matsuo, M. Tyagi, and J. Sugiyama, *J. Phys. Soc. Jpn.* **83**, 074604 (2014).
- [30] M. C. Verbraeken, C. Cheung, E. Suard, and J. T. S. Irvine, *Nat. Mater.* **14**, 95 (2015).
- [31] K. Fukui, S. Iimura, T. Tada, S. Fujitsu, M. Sasase, H. Tamatsukuri, T. Honda, K. Ikeda, T. Otomo, and H. Hosono, *Nat. Commun.* **10**, 2578 (2019).
- [32] H. Ubukata, F. Takeiri, K. Shitara, C. Tassel, T. Saito, T. Kamiyama, T. Broux, A. Kuwabara, G. Kobayashi, and H. Kageyama, *Sci. Adv.* **7**, eabf7883 (2021).
- [33] F. Takeiri, A. Watanabe, K. Okamoto, D. Bresser, S. Lyonnard, B. Frick, A. Ali, Y. Imai, M. Nishikawa, M. Yonemura, T. Saito, K. Ikeda, T. Otomo, T. Kamiyama, R. Kanno, and G. Kobayashi, *Nat. Mater.* **21**, 325 (2022).
- [34] T. Liang, Z. Zhang, H. Yu, T. Cui, X. Feng, C. J. Pickard, D. Duan, and S. A. T. Redfern, *J. Phys. Chem. Lett.* **12**, 7166 (2021).
- [35] C.-s. Zha, H. Liu, J. S. Tse, and R. J. Hemley, *Phys. Rev. Lett.* **119**, 075302 (2017).
- [36] A. Jayaraman, *Phys. Rev.* **139**, A690 (1965).
- [37] M. Millot, S. Hamel, J. R. Rygg, P. M. Celliers, G. W. Collins, F. Coppari, D. E. Fratanduono, R. Jeanloz, D. C. Swift, and J. H. Eggert, *Nat. Phys.* **14**, 297 (2018).
- [38] G. Weck, J.-A. Queyroux, S. Ninet, F. Datchi, M. Mezouar, and P. Loubeyre, *Phys. Rev. Lett.* **128**, 165701 (2022).
- [39] Z. Zhang, T. Cui, M. J. Hutcheon, A. M. Shipley, H. Song, M. Du, V. Z. Kresin, D. Duan, C. J. Pickard, and Y. Yao, *Phys. Rev. Lett.* **128**, 047001 (2022).
- [40] T. Meier, F. Trybel, G. Criniti, D. Laniel, S. Khandarkhaeva, E. Koemets, T. Fedotenko, K. Glazyrin, M. Hanfland, M. Bykov, G. Steinle-Neumann, N. Dubrovinskaia, and L. Dubrovinsky, *Phys. Rev. B* **102**, 165109 (2020).
- [41] A. Stukowski, *Modelling Simul. Mater. Sci. Eng.* **18**, 015012 (2010).
- [42] A. Kokalj, *J. Mol. Graphics Modelling* **17**, 176 (1999).